

Transducin-Deficient Rod Photoreceptors Evaluated With Optical Coherence Tomography and Oxygen Consumption Rate Energy Biomarkers

Bruce A. Berkowitz,¹ Robert H. Podolsky,² Karen Lins Childers,³ Robin Roberts,¹ Ryan Katz,¹ Rida Waseem,¹ Brian M. Robbings,^{4,5} Daniel T. Hass,⁴ James B. Hurley,⁴ Ian R. Sweet,⁵ Cole Goodman,¹ Haohua Qian,⁶ Bruno Alvisio,⁷ and Sam Heaps⁷

¹Department of Ophthalmology, Visual and Anatomical Sciences, Wayne State University School of Medicine, Detroit, Michigan, United States

²Biostatistics and Study Methodology, Children's National Hospital, Silver Spring, Maryland, United States

³Beaumont Research Institute, Beaumont Health, Royal Oak, Michigan, United States

⁴Department of Biochemistry, Department of Ophthalmology, University of Washington, Seattle, Washington, United States

⁵Department of Medicine, UW Medicine Diabetes Institute, University of Washington, Seattle, Washington, United States

⁶Visual Function Core, National Eye Institute, National Institutes of Health, Bethesda, Maryland, United States

⁷OSIO Bioinformatics Core, National Eye Institute, National Institutes of Health, Bethesda, Maryland, United States

Correspondence: Bruce A. Berkowitz, Wayne State University School of Medicine, 540 E. Canfield, Detroit, MI 48201, USA; baberko@med.wayne.edu.

Received: August 26, 2022

Accepted: December 5, 2022

Published: December 28, 2022

Citation: Berkowitz BA, Podolsky RH, Childers KL, et al. Transducin-deficient rod photoreceptors evaluated with optical coherence tomography and oxygen consumption rate energy biomarkers. *Invest Ophthalmol Vis Sci.* 2022;63(13):22. <https://doi.org/10.1167/iovs.63.13.22>

PURPOSE. To test the hypothesis that rod energy biomarkers in light and dark are similar in mice without functional rod transducin (Gnat1^{rd17}).

METHODS. Gnat1^{rd17} and wildtype (WT) mice were studied in canonically low energy demand (light) and high energy demand (dark) conditions. We measured rod inner segment ellipsoid zone (ISEZ) profile shape, external limiting membrane–retinal pigment epithelium (ELM-RPE) thickness, and magnitude of a hyporeflexive band (HB) intensity dip located between photoreceptor tips and apical RPE; antioxidants were given in a subset of mice. Oxygen consumption rate (OCR) and visual performance indexes were also measured.

RESULTS. The lower energy demand expected in light-adapted wildtype retinas was associated with an elongated ISEZ, thicker ELM-RPE, and higher HB magnitude, and lower OCR compared to high energy demand conditions in the dark. Gnat1^{rd17} mice showed a wildtype-like ISEZ profile shape at 20 minutes of light that became rounder at 60 minutes; at both times, ELM-RPE was smaller than wildtype values, and the HB magnitude was unmeasurable. OCR was higher than in the dark. Light-adapted Gnat1^{rd17} mice biomarkers were unaffected by anti-oxidants. Gnat1^{rd17} mice showed modest outer nuclear layer thinning and no reduction in visual performance indexes.

CONCLUSIONS. Light-stimulated changes in all biomarkers in WT mice are consistent with the established light-induced decrease in net energy demand. In contrast, biomarker changes in Gnat1^{rd17} mice raise the possibility that light increases net energy demand in the absence of rod phototransduction.

Keywords: photoreceptor, OCT, energy, OCR

The *GNAT1* gene encodes for the α subunit of transducin 1, a key component of rod photoreceptor cell phototransduction.^{1,2} Mutations in *GNAT1*, such as Intron 4 deletion leading to Tyr150*, prevent G-protein activation and cause rod photoreceptor degeneration in humans as a form of retinitis pigmentosa, a condition reproduced in mice with similar mutations (e.g., Gnat1^{rd17}; see <http://www.informatics.jax.org/allele/MGI:3707708> for more details).¹⁻⁹ We reasoned that because transducin 1 loss-of-function prevents rod phototransduction, the rod energy demands in light-adapted mice may resemble that in dark-adapted mice. On the other hand, Gnat1^{rd17} mice exhibit a mild rod photoreceptor degeneration.^{4,10-15} Rod mitochondria activ-

ity can chronically decrease or increase in rod degeneration models with different mutations, and it is unclear how the rod energy ecosystem changes in the Gnat1^{rd17} mice.¹⁵⁻²¹ Given the clinical relevance of Gnat1^{rd17} mice, we asked whether there is biomarker evidence for rod mitochondria under- or overperforming, conditions likely requiring different treatment strategies to mitigate their rod degeneration.¹⁻⁹

Currently, it is difficult to evaluate mitochondria activity in vivo using conventional functional imaging modalities, such as magnetic resonance imaging (MRI) or positron emission tomography.²²⁻²⁵ Optical coherence tomography (OCT) offers a potential solution to this problem. For example,

the profile shape of a hyperreflective band in the outer retina (also called “band 2”) immediately posterior to the external limiting membrane (ELM), a feature that is easily identified with commercial clinical and animal OCT systems. Band 2 has been called the inner segment ellipsoid zone (ISEz) in a consensus clinical lexicon with a body of supporting literature.^{26–29} Our studies have found agreement between light-dark mitochondria distribution within the inner segment ellipsoid measured from electron microscopy and OCT in wildtype mice with different mitochondria activity.²³ Based on these data, and the fact that mitochondria scatter light, we interpret the ISEz profile shape as a functional biomarker of rod mitochondria spatial arrangements; for a possible alternative interpretation of band 2, see Discussion (below). In addition, we also measure the thickness of the ELM to the retinal pigment epithelium (RPE) region, which decades of research have shown to be modulated by mitochondrial-driven/pH-triggered/RPE-water removal from the subretinal space; changes in ELM-RPE thickness have been reported in animal models and in humans for both rods and cones.^{23,24,30–54} A less understood index is the signal magnitude of a hyporeflexive band (HB) between the tips of the photoreceptors and apical RPE. The HB magnitude refers to the absolute value of the peak reflectance amplitude from baseline drawn between the photoreceptor tips and RPE layer; the HB has arbitrary units as indicated on the y-axis as “a.u.” The HB index shows energy-dependent changes that are correlated with ELM-RPE changes in control mice but does not seem to be triggered by pH changes.²⁴ Agreement between these OCT energy biomarkers and direct read-outs of metabolic activity, including ATP levels, has been found.^{24,30–34}

In this study, we examined Gnat1^{rd17} mice at two months of age, a time when there is little reported histologic evidence for retinal degeneration in fixed tissue; at six months of age and older, progressive histologic loss of rod cells occurs.^{3,55} However, it is unclear whether there is evidence in vivo for rod loss or dysfunction earlier than six months. Here we use analytic OCT approaches to test this notion. Cone-based visual performance was tested by optokinetic tracking, which is also sensitive to outer retina dysfunction.^{56–58} Although not studied herein, we note that retinas without rod transducin 1 α -subunit (*Gnat1*^{-/-}) exhibit oxidative stress, a condition that can modify pH and has been shown to induce ELM-RPE thinning in light-adapted mice.^{31,59,60} In this study, we compared the three OCT biomarkers in Gnat1^{rd17} mice given saline solution or antioxidants (i.e., QUEnch-assISTed [QUEST] OCT).⁶⁰ Finally, as an independent test of the OCT bioenergy biomarker results, measurements of the O₂ consumption rate (OCR) were performed as a conventional reporter of the oxidative biochemical activities in mitochondria that release energy from fuels.

METHODS

All mice were treated in accordance with the National Institutes of Health Guide for the Care and Use of Laboratory Animals, the Association for Research in Vision and Ophthalmology Statement for the Use of Animals in Ophthalmology and Vision Research, and with specific authorization by the Wayne State University and University of Washington Division of Laboratory Animal Resources Institutional Animal and Care Use Committees (IACUC). For all studies, two-month-old wildtype and Gnat1^{rd17} C57BL/6J mice

(JAX:000664 and 008811, respectively; Jackson Laboratories, Bar Harbor, ME, USA) were housed and maintained in 12-hour:12-hour light/dark cycle laboratory lighting. At Wayne State University mice were humanely euthanized by an overdose of ketamine/xylazine followed by cervical dislocation, per an IACUC-approved protocol. At the University of Washington, mice for OCR measurements were euthanized by awake cervical dislocation following an IACUC-approved protocol.

Optokinetic Tracking

Using optokinetic tracking (OKT), two visual performance index were evaluated from freely moving mice: spatial frequency thresholds (SFT, “acuity,” in cycles/deg [c/d]) and contrast sensitivity, measured at the peak of the nominal curve [0.06 cycles/deg], inverse Michelson contrast [unitless] (OptoMotry; CerebralMechanics, Inc., Alberta, Canada), an established method.^{61–63} In our laboratory, acuity and peak of contrast sensitivity for each mouse was measured over a 30-minute time period; in our experience, mice tend to be uncooperative in the afternoon, so OKT was performed before noon. Given the similarity in OCT results between male and female mice (Supplemental Figs. S2, S4), OKT studies were limited to male wildtype and Gnat1^{rd17} mice. Note that OKT has no spatial resolution, and its response is strongly weighted toward those parts of the retina with more cones. Although there is widespread distribution of cones with M- and S-opsin (with modest heterogeneity), loss of function of either, or both, would be expected to decrease visual performance indices.^{64,65}

OCT

Using a cross-sectional design, mice were first dark-adapted overnight and then either room light-adapted for 20 minutes or 60 minutes the following day before imaging, or dark-adapted overnight and studied in the dark the following day. The 60-minute time was chosen because it produces a large ISEz profile shape difference between light and dark conditions in wildtype C57BL/6J mice (data not shown).²³ To compare to the 20-minute time point of the OCR experiment, OCT studies were repeated at a 20-minute time point. As noted below, at longer times, OCR studies of ex vivo retina without RPE are expected to prevent rhodopsin regeneration and not best represent in vivo conditions; although not germane to the present study, we note that functional OCT studies that occur on a time scale of seconds or shorter are reported to measure small deformations in individual cone photoreceptor cells because of isomerization of photopigment and thus do not involve the RPE.^{66–68} Examinations were performed before noon with an Envisu UHR2200 OCT (Bioptigen) which has an axial resolution of 1.8 μ m. Anesthesia with ketamine (100 mg/kg) and xylazine (6 mg/kg) (Sigma-Aldrich, St. Louis, MO, USA), pupillary dilation (1% atropine sulfate) was administered 15 minutes before OCT examination, and corneal hydration (Systane Ultra) was performed as described previously. Our acquisition parameters are radial volume scan, A-scans/B-scans = 1000 lines; B-scans/volume = 1000 scans; Frames/B-scan = 1 frame. B scan numbers 450 to 549 representing inferior-superior central retina sampled out to 624 μ m from the optic nerve head, were extracted, and these 100 images were registered and averaged using an R script (summarized in Fig. 1).⁵⁶

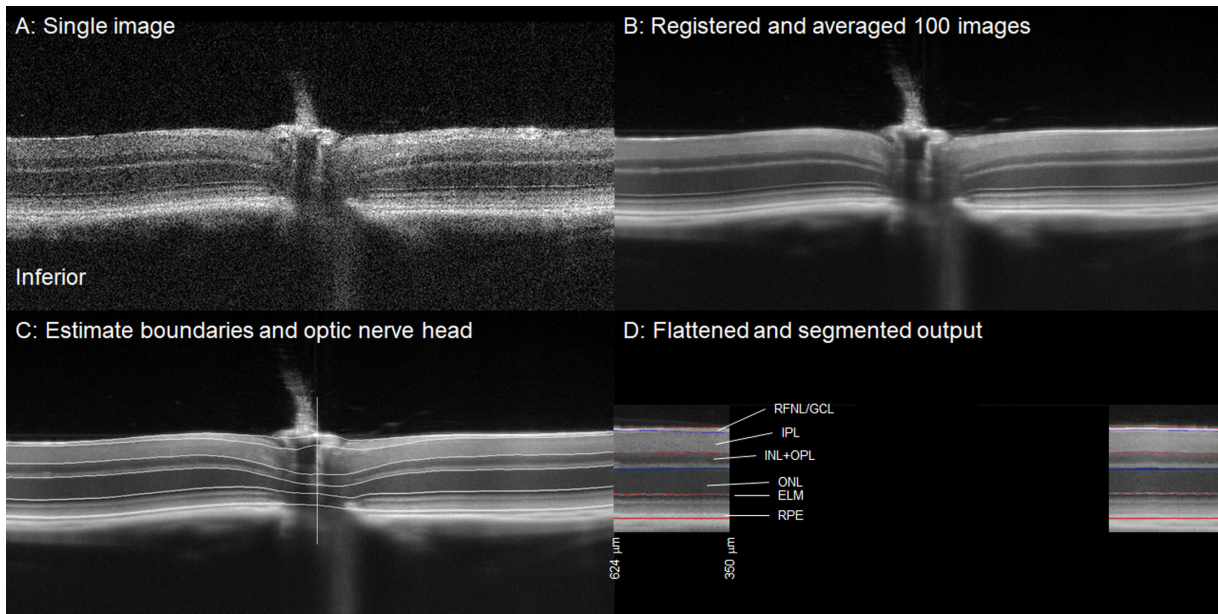


FIGURE 1. Image preparation pipeline. **(A)** A single inferior-superior central retina slice versus **(B)** 100 such slices extracted from the radial scans, registered, and averaged demonstrating improved signal-to-noise. **(C)** Example of estimated laminar boundaries and optic nerve head identification used as input to an R script that will produce a final **(D)** flattened and segmented image (alternating *red* and *blue* lines used for clarity). Note only the information for regions between 350 and 624 μm were used for further analysis (non-analyzed regions blacked out). RFNL/GCL, retinal nerve fiber layer/ganglion cell layer; IPL, inner plexiform layer; INL + OPL, inner nuclear layer + outer plexiform layer.

Layers were segmented by first estimating boundaries, either manually or from a machine learning model-based computer program. The machine learning model was a U-net convolutional neural network trained using the “dice loss” function and the Adam optimizer (learning rate = 0.001), with 665 previously labeled images for training and 166 and 356 images for validation and testing, respectively.⁶⁹ To improve the model’s performance, its predictions were post-processed by applying a shortest-path algorithm.⁷⁰ From either the manually drawn or model-based estimates, the segmentation estimates were then processed with another R script to segment the image and extract the output indexes described below. In a representative example, we entered the same OCT data after either manual or model-based boundary estimates into the R script; the output for all three biomarkers were nearly identical showing support for use of either estimate (Supplemental Fig. S1). A representative image and set of axial reflectance profiles are shown in Figure 2. The intensity values used to generate the ISez shape profile are measured from a log-based image with a 16-bit depth (default in the Bioptigen system); our preliminary analysis suggested that both scales generate, for example, similar ISez profile shapes and standard deviations.²³

Inferior and superior retina (350 to 624 μm from the optic nerve head on the inferior and superior sides) were each analyzed; starting at 350 μm ensured that our data were analyzed away from the optic nerve head, where the outer retina is relatively uniform in all OCT data (Fig. 1). After estimating the boundaries, we run an in-house-generated R script that generates several key outputs: (1) a spreadsheet of distances from the optic nerve head and layer thickness, (2) an “RAS” (short for registered and stretched) image that has been spatially normalized (stretched) to align layers. The R code uses fiduciary points to do this. The program assigns 12 points from $-30 \mu\text{m}$ to $0 \mu\text{m}$ from the choroid to the

RPE (inclusive of lower value and upper, all others are inclusive of upper value only, so the next line starts one step beyond RPE, and lands on ELM); assigns 38 points to the RPE-ELM span; assigns 36 points to the ELM-outer nuclear layer (ONL)/outer plexiform layer (OPL span; assigns 36 points to the ONL/OPL – INL + inner plexiform layer (IPL) span; assigns 50 points to the INL + IPL – RNFL/GCL span; assigns 18 points to the RNFL/GCL – retina/vitreous border span; and assigns 10 points from the retina/vitreous border to $30 \mu\text{m}$ into the vitreous. Together, there are 200 points that slightly over-represent the outer retina span the region of interest. (3) An R output that generates a spreadsheet containing the HB magnitude. An additional output image that was not stretched, referred herein as an NS image, is also generated in which only the basal aspect of the RPE is aligned without stretching the image; this image is used to generate the transretinal A-line profiles shown in the figures.

The advantage of using the RAS format is that the ISez is positioned in the same place for each image; in preliminary studies in wildtype mice, agreement was found between RAS-based ISez profile shape and those calculated from NS images; it is possible that in models with a large extent of rod loss, the ISez aspect ratio using RAS and NS images will be somewhat different (not shown). To generate the ISez profile shape, the RAS image is resized to a width of 100 pixels and a height of 259 pixels using a bilinear interpolation; signal intensity is also set to a fixed value (ImageJ macro). A fixed size region-of-interest is then positioned to span 350 to 624 μm from the optic nerve head on the inferior or superior sides using two separate ImageJ macros (Fig. 1). These steps are performed to take advantage of a built-in function within ImageJ (“Plot lanes”) for drawing profiles. Next, a baseline is hand drawn and the wand feature used to define the ISez region of interest. The shape of this ISez is then summarized using the “Fit Ellipse” option.

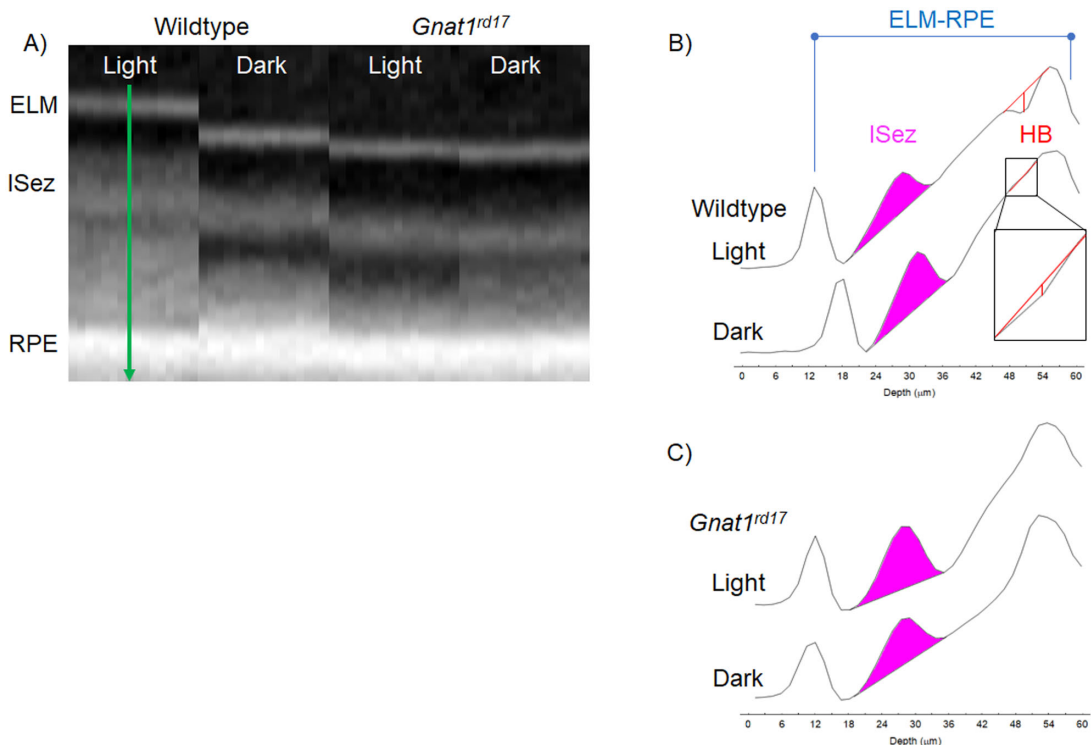


FIGURE 2. Comparative OCT B-scans and corresponding A-line profiles from both strains under light/dark conditions. **(A)** Representative OCT of inferior outer retina for light-dark wildtype and $Gnat1^{rd17}$ mice. *Green arrow*: direction of A-line profiles in B). **(B)** Average superior A-line profiles from images shown in A) for 60 minute light-adapted wildtype ($n = 5$ per condition; *top*) and a $Gnat1^{rd17}$ ($n = 5$ per condition; *bottom*) mice; zoomed-in region of the dark wildtype data is shown in the *black box* to illustrate the smaller HB magnitude. The ISez (*pink*), ELM-RPE (*blue*), and HB (*red*) indexes are shown. The light-adapted $Gnat1^{rd17}$ mouse has a visibly rounder ISez, thinning of its ELM-RPE region, and no discernable HB signal compared to the light-adapted wildtype mouse; together these biomarkers raise the possibility of a higher energy demand condition in $Gnat1^{rd17}$ rod mitochondria; other interpretations are possible (see Discussion). No upsampling/zero-filling is used for the A-line profiles.

In the results window, the value under the column marked “round” is the minor/major aspect ratio for the fitted ellipse. The ISez profile shape (i.e., OCT signal magnitude along the length of the ISez [illustrated in Fig. 2B] was extracted using ImageJ macros).⁷¹ The magnitude values used to generate the ISez shape profile are from the Bioptigen system.²³ The ISez profile shape was converted into an ellipse with the same area and its minor/major aspect ratio determined; this process is described here <https://imagej.nih.gov/ij/source/ij/process/EllipseFitter.java> and more formally in the literature.⁷² In this study, we chose to use the best-fit ellipse aspect ratio, a commonly used shape descriptor; whether it is an optimal shape description for the ISez profile shape is not yet clear.⁷²

As summarized in Figure 2, two other biomarkers (i.e., ELM-RPE thickness and magnitude of the HB signal intensity; described in detail elsewhere and summarized in Fig. 2B) were generated from in-house R scripts, as previously described.^{25,73–75} A straight line is drawn between the RPE and the outer segment tip portions of the profile (intersecting only one point on each side of HB) and the largest departure from that line is the magnitude of the HB signal magnitude (i.e., the absolute value of the signal intensity dip from baseline; see Fig. 2); more work is needed to determine whether other approaches for calculating the HB magnitude provide any additional benefits.^{13,24,32}

QUEST OCT was performed as follows. Methylene blue was given IP 24 hours before OCT and is an alternate electron transporter that effectively suppresses generation of superoxide; α -lipoic acid was given one hour before

OCT as a potent free radical neutralizer; both are approved by the Food and Drug Administration and have been shown to be useful in several QUEST studies.^{14,60,76–79} Please note that freeware R scripts and ImageJ macros for all of the above procedures are provided as Supplemental Material 2 (available here <https://github.com/baberko/Supplemental-material-2>).

Ex Vivo OCR Measurements

OCR rate measurements with isolated retina are a conventional assay for evaluating retinal metabolic activity.^{15,33,80–83} OCR is thus helpful as a discovery/companion assay but naturally comes with limitations for applicability to the in vivo situation (see Discussion). Female mice seven to 11 weeks old were dark-adapted overnight. All procedures were carried out in the complete absence of visible light using night vision goggles and infrared illumination. The mice were euthanized by awake cervical dislocation. Intact retinas were isolated from each euthanized mouse immediately. The retinas were incubated in Krebs-Ringer bicarbonate buffer (KRB) supplemented with 5 mM glucose and pre-equilibrated at 37°C and 5% CO₂. We used a custom-built perfusion flow-culture system to measure OCR.⁸² Retinas had Cytopore beads (Amersham Biosciences, Piscataway, NJ, USA) and porous frits above and below them in chambers that were perfused with KRB supplemented with 5 mM glucose, 1× Antibiotic-Antimycotic (Gibco, Thermo Fisher Scientific, Waltham, MA, USA), and 1 mg/mL bovine serum albumin. KRB was equilibrated to

a gas mixture of 21% O₂, 5% CO₂, and 74% N₂ using an artificial lung. Tissue was equilibrated in the system 90 minutes before acquiring OCR data. Outflow media flowed past a thin layer of O₂-sensitive polymerized Pt(II) Meso-tetra(pentafluorophenyl)porphine dye (PtT975; Frontier Scientific, Logan, UT, USA) painted on the inner glass wall of the chamber. A 405 nm light pulse stimulated the dye to emit a phosphorescent signal detected at 650 nm. The light source was isolated from the chamber so that it could not stimulate the retina. The decay lifetime of the dye depends on O₂ tension. We determined OCR from the flow rate along with the quantitative relationship between dye phosphorescent decay and O₂ concentration.⁸⁴ There were 4 whole retinas in each chamber (a single replicate) with a flow rate of 80 to 85 μ L/min; 290 lux was measured at the surface of the sample chamber. The zero OCR baseline for calibration was determined by adding 3 mM KCN to inhibit complex IV activity. This value was subtracted to eliminate any residual non-mitochondrial O₂ consumption. Finally, fractional OCR is calculated by dividing individual OCR values over time by the average value of the baseline before the start of the experimental conditions so that the baseline is equal to 1 and all other values are a fraction of the baseline. Given the similarity in OCT results between male and female mice (Supplemental Figs. S2, S4), OCR studies were limited herein to female wildtype and Gnat1^{rd17} mice.

Statistical Analysis

Data are presented as mean and 95% confidence intervals. All outcomes (OKT, ISez aspect ratio, hyporeflexive band magnitude, OCT layer thickness, and fractional OCR) had repeated measures for each mouse. As such, we used mixed models to analyze all outcomes using the Kenward-Roger method for calculating degrees of freedom in either PROC MIXED or PROC GLIMMIX of SAS/STAT software. We used linear contrasts for all comparisons based on the final model. A significance level of 0.05 was used for most tests, with interactions being tested using a significance level of 0.10 because of these tests having less power. For all models, higher-order interactions were evaluated first and removed if not significant until all interactions included in the model were either significant or removed from the model. Overall, within-mouse variation in these profiles is small relative to the between-mouse variation in profiles. Hence, we elect to analyze averages.

For OKT, SFT and contrast sensitivity were analyzed similarly, but assuming different data distributions. We assumed that SFT was normally distributed, and we used a gamma-link in a generalized linear mixed model for contrast sensitivity. For both measurements, the initial model included the fixed effects of strain (WT and Gnat1^{rd17}), rotation (CW and CCW), a strain by rotation interaction, and a random intercept for mouse nested within strain. The models were fit using PROC GLIMMIX.

We used the same modeling strategy for ISez aspect ratio shape, OCT retinal layer thickness, and magnitude of hyporeflexive band magnitude. Before fitting the OCT models, we first averaged thickness measured 350 to 624 μ m from the optic nerve head on either side for each mouse within each layer (ELM-RPE, ONL, INL + OPL, IPL, and RNFL). For 60-minute light-adapted mice, the models included the fixed effects of light condition (light vs. dark), side (inferior vs. superior), strain (WT vs. Gnat1^{rd17}), sex (male vs. female), all interactions, and a random intercept

for mouse within light condition, strain, and sex. Because only male mice were included in the 20-minute light-adapted study, the models included the fixed effects of light condition, side, strain, all interactions, and a random intercept for mouse within light condition and strain. We evaluated whether residual variances depended on light condition, strain, or sex (if applicable) using the Akaike and Schwarz Bayesian information criteria (AIC and BIC). None of the outcomes showed a decrease in either AIC or BIC greater than 10 leading us to assume the residual variance was constant across light condition, strain, and sex. We used Tukey's honestly significant difference to adjust for multiple comparisons among all strain/light condition groups. The models were fit using PROC MIXED.

Fractional OCR was measured over time resulting in an OCR profile. We used restricted cubic splines to model and compare mouse-specific profiles between strains. This method fits separate cubic regressions within a set number of "windows" with the boundaries of the windows determined by knot locations, and the lines in adjacent windows constrained to be continuous across windows. The number of windows with a relationship between outcome and time (i.e., knots) was initially evaluated separately for each strain (WT and Gnat1^{rd17}) using AIC and BIC to identify the model with the fewest knots needed to model each strain. Random coefficients for the intercept and time-specific coefficients (cubic spline coefficients) with mouse nested within strain were also evaluated using AIC and BIC. We used an unstructured covariance matrix for the random coefficients to account for associations in spline coefficients because of subject-specific profiles. The model used 10 knots, included the fixed effects of strain, time-specific values for the cubic splines, two-way interactions among strain and the spline coefficients, and random coefficients for the intercept, time and the first knot coefficient. The models were fit using PROC MIXED.

RESULTS

OKT Evaluation

As expected, Gnat1^{rd17} mice did not have diminished acuity or contrast sensitivity under photopic illumination condi-

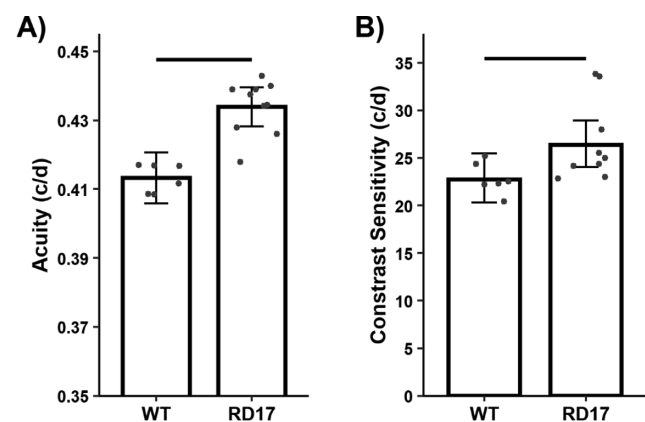


FIGURE 3. Summary of visual performance in controls (WT) and Gnat1^{rd17} (rd17) mice. Greater-than-normal (A) acuity and (B) contrast sensitivity are noted in Gnat1^{rd17} mice (n = 5 WT, n = 5 Gnat1^{rd17}). Black horizontal line: $P < 0.05$; mean \pm 95% CI. n = 5 WT, n = 5 Gnat1^{rd17}.

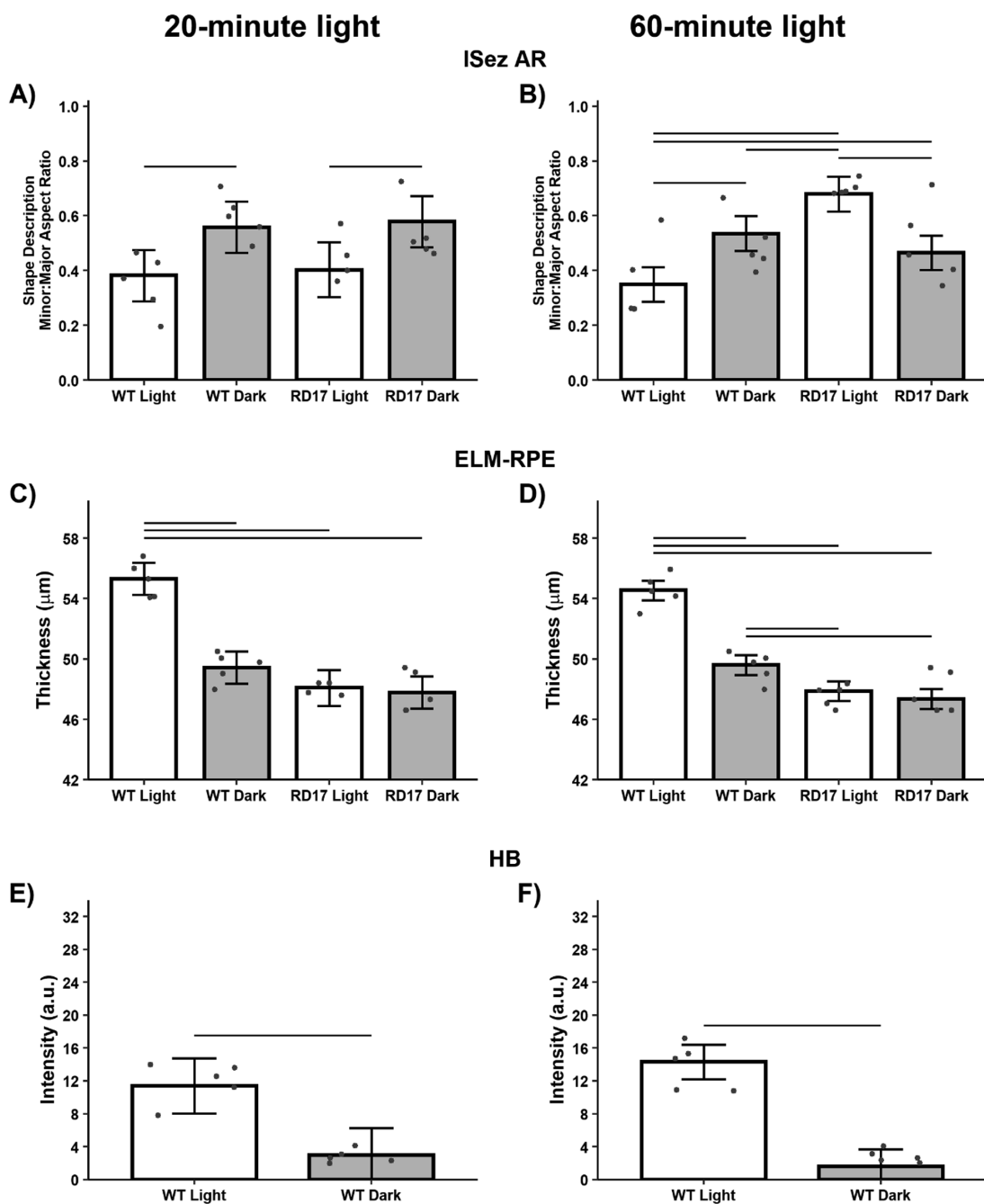


FIGURE 4. Summary of 20 minutes (left column) versus 60 minutes (right column) light (*white*), and dark (*black*) changes in bioenergy OCT biomarkers from WT and *Gnat1*^{rd17} mice (rd17). Note that only superior side for males is shown; inferior male results, and inferior and superior female results were all similar (see supplemental material for full data set). *Black horizontal line:* $P < 0.05$; mean \pm 95% CI, $n = 5$ WT, $n = 5$ *Gnat1*^{rd17} per time point.

tions compared to age- and strain-matched controls (Fig. 3), consistent with the expected intact cone function. However, *Gnat1*^{rd17} mice exhibited modest and significant, greater-than-normal visual performance indexes.

Rod OCT Bioenergy Biomarkers

Next, we noninvasively investigated outer retina biomarkers in light and dark-adapted wildtype and *Gnat1*^{rd17} mice.

Our previous studies indicate that these correlate to retina energetic status in wildtype mice.²³⁻²⁵

OCT ISez Profile Shape. We reported previously that the ISez profile shape measured from OCT data mirrors the distribution of mitochondria within the IS ellipsoid.²³ In 20- or 60-minute light-adapted wildtype controls, a more elliptical ISez aspect ratio in low-energy demand conditions was found, compared to the rounder ISez aspect ratio in high-energy demand conditions (i.e., dark) (Figs. 4A, 4B; Supplemental Fig. S2). *Gnat1*^{rd17} mice at 20 minutes of light

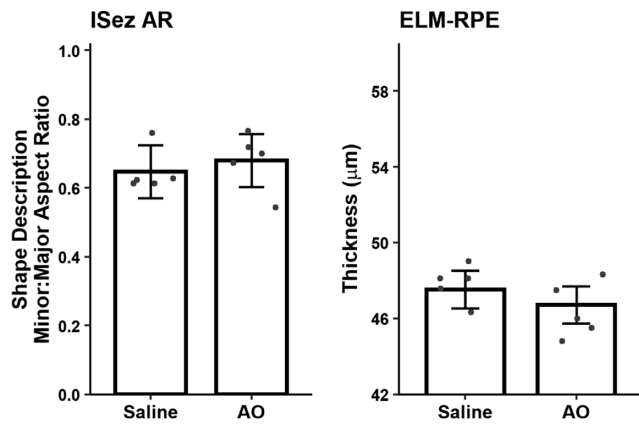


FIGURE 5. Summary of light \pm saline or antioxidants (AO) did not change bioenergy OCT biomarkers of $Gnat1^{rd17}$ mice. Note, that inferior and superior values were not significantly different; thus average side results are shown (see supplemental material for full data set); $n = 5$ $Gnat1^{rd17}$ mice + saline; $n = 5$ $Gnat1^{rd17}$ mice + AO.

produced a similar ISez profile shape pattern to that in light-adapted controls (Fig. 4A). However, at 60 minutes of light, $Gnat1^{rd17}$ mice produced an opposite light-dark profile shape pattern (Fig. 4B). This light-dark difference was largely due to $Gnat1^{rd17}$ mice having a rounder ISez aspect ratio than controls in the light (Figs. 4A and B). It is possible that as rods die, the energy needs of the cell will decrease in tandem. In this case, the ratio of ISez to ONL thickness would remain the same. However, after dividing the ISez by ONL thickness for each mouse to normalize to different ONL layer thicknesses, we still observed a rounder ISez in $Gnat1^{rd17}$ mice than wildtypes in the light (data not shown), suggesting that rod loss per se in the $Gnat1^{rd17}$ mice did not account for the ISez difference. Nonetheless, the onset of retinal degeneration preceded the time point of the experiments, so it cannot be definitely concluded that a rounder ISez in $Gnat1^{rd17}$ mice is due solely to *Gnat1* loss-of-function. To investigate these changes in profile shape and to explore their relationships to energy demand and production, we examined two additional OCT bioenergy indexes for physi-

ologic consequences of this presumptive change in rod mitochondria distribution in $Gnat1^{rd17}$ mice.

Rod ELM-RPE Thickness and Magnitude of the HB Signal Intensity. In 20- and 60-minute light-adapted WT controls, ELM-RPE is thicker than in the dark (Figs. 4C, 4D, Supplemental Fig. S2). However, in $Gnat1^{rd17}$ mice, no light-dark difference was measured at either time point (Figs. 4C, 4D). This lack of a difference was largely due to $Gnat1^{rd17}$ mice having a thinner ELM-RPE than controls in the light (Figs. 4C, 4D); only at the 60-minute time point was a modest reduction in ELM-RPE thickness noted in dark (Figs. 4C, 4D).

In 20- or 60-minute light-adapted WT controls, HB magnitude was greater than in the dark (Figs. 4E, 4F, Supplemental Fig. S2). The HB magnitude in $Gnat1^{rd17}$ mice was about zero, as shown in Figure 2, in the 20- and 60-minute light and in the dark.

QUEST OCT. Outer retinal oxidative stress has not been documented in $Gnat1^{rd17}$ mice but has been shown in *Gnat1* knockout mice.^{31,59,60} To check for an impact of potential oxidative stress on our OCT biomarkers in the present study, we examined $Gnat1^{rd17}$ mice given either saline or anti-oxidants (i.e., methylene blue and α -lipoic acid) that have been shown to robustly reduce excessive production of reactive oxygen species in other models.^{14,60,76-79} Oxidative stress can impact at least one of the parameters measured in this study, light-dark ELM-RPE thickness difference.^{31,59,60} At the time of largest changes in OCT biomarkers (i.e., 60-minute), the ISez profile shape and ELM-RPE thickness in light-adapted male $Gnat1^{rd17}$ mice were unresponsive to antioxidant treatment (Fig. 5, Supplemental Fig. S3) suggesting the absence of oxidative stress.⁶⁰

Retinal Laminar Thickness. $Gnat1^{rd17}$ mice showed modest and significant thinning localized to the ONL; the thickness of INL+OPL layers were greater than normal and was unremarkable in the other layers (Fig. 6, Supplemental Fig. S4).

OCR. To independently test our interpretation of the OCT biomarkers, that in the light $Gnat1^{rd17}$ mice increase rather than decrease mitochondrial activity, OCR was performed. There was no significant difference in baseline OCR in darkness between retinas from dark-adapted control and $Gnat1^{rd17}$ mice (1.20 nmol O_2 per minute per

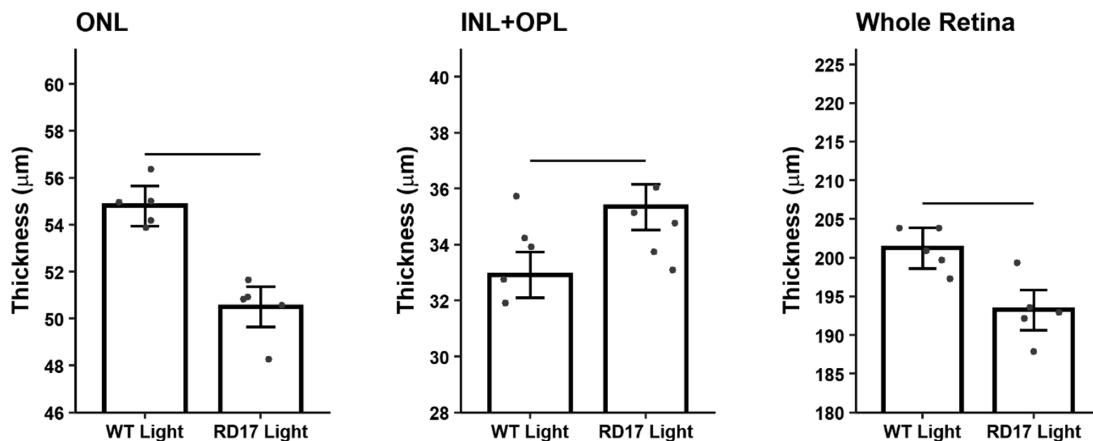


FIGURE 6. Summary of retinal layer changes between male controls (WT, $n = 5$) and $Gnat1^{rd17}$ (rd17, $n = 5$) mice; results between sides, 20-minute and 60-minute light, and between light and dark, were similar and only average sides at 60-minute light are shown for clarity (see supplemental material for full data set). Compared to controls, $Gnat1^{rd17}$ showed laminar thinning for ONL but not INL + OPL. *Black horizontal line:* $P < 0.05$; mean \pm 95% CI.

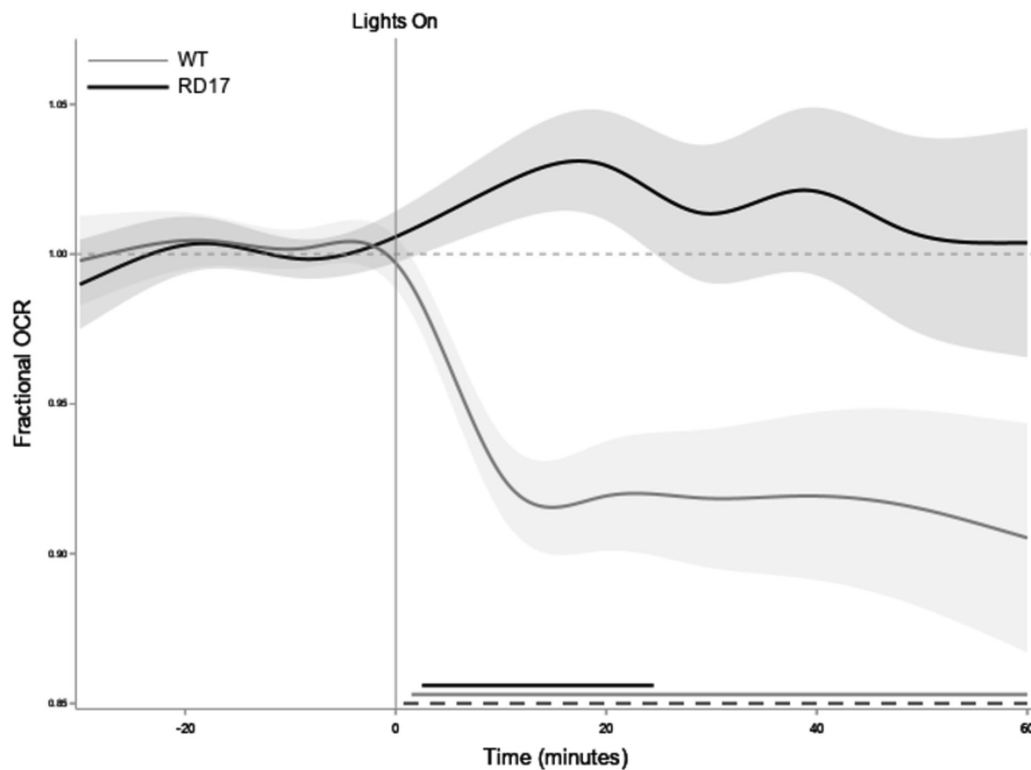


FIGURE 7. Summary of fractional OCR under dark (negative times) and light (positive times) for WT (*thin gray bar* = mean; 95% CI shown) and $Gnat1^{rd17}$ (*thick black bar* = mean) mice. *Dotted horizontal line* at 1 presented for reference. Statistical test results shown in bottom right: *Horizontal lines*: $P < 0.05$; mean \pm 95% CI. $Gnat1^{rd17} \neq 1$; *gray solid bar* WT $\neq 1$; *dashed line* $Gnat1^{rd17} \neq$ WT; $n = 4$ at each condition for WT and $Gnat1^{rd17}$ mice.

retina \pm 0.17 SEM for four control retinas and 1.02 nmol O_2 per minute per retina \pm 0.23 SEM for 4 $Gnat1^{rd17}$ retinas). As expected, exposure of dark-adapted retinas from WT control mice to constant illumination consistently slows OCR (Fig. 7). However, exposure of dark-adapted retinas from $Gnat1^{rd17}$ mice to constant illumination produced a modest and significant increase in OCR above dark-levels.

DISCUSSION

The OCT and OCR biomarker data in this study raise the possibility that rod mitochondrial activity is greater in light-adapted loss-of-function of transducin 1 mice (a model that mirrors some forms of retinitis pigmentosa in humans) than in the dark.¹⁻⁹ A limitation of all noninvasive bioenergy biomarkers, including the results herein, is that rod mitochondria are not being isolated and directly interrogated by anatomical, physiological, or genetic approaches. On the other hand, such ex vivo methods are not useful in patients, and it is unclear how to translate results from bench-to bedside. To address this need to translate ex vivo results in vivo, studies in wildtype mice have developed and applied noninvasive OCT energy biomarkers that are sensitive to changes in mitochondria activity.²³⁻²⁵

In this study, we begin to test the usefulness of these biomarkers in $Gnat1^{rd17}$ mice, which lack rod phototransduction and model a form of human retinitis pigmentosa.¹⁻⁹ At 60 minutes of light, $Gnat1^{rd17}$ mice show a rounder ISez, together with a thinner ELM-RPE and unmeasurable HB magnitude compared to wildtype mice, a totality of change suggesting that $Gnat1^{rd17}$ rod mitochondria have altered

their distribution to increase energy demand.²³ The lack of an elevated ISez aspect ratio at 20 minutes of light together with ELM-RPE thinning and lack of HB signal is not inconsistent with the notion of mitochondria overperformance, but it is somewhat ambiguous (see below). One alternative way that mitochondria can change energy output without spatial rearrangements is by changing the expression pattern of OPA1 on the inner mitochondria membrane, a major regulator of mitochondrial homeostasis and cristae remodeling; this change would not be discernable with OCT and is a hypothesis that needs to be formally tested.^{85,86} It is also possible that modest mitochondria spatial changes occurred at 20 minutes that were below our detection sensitivity. We thus did an OCR “tie-breaker” experiment. The OCR results supported a greater-than-dark energy performance in the light from retina’s of $Gnat1^{rd17}$ mice consistent with the ELM-RPE and HB biomarkers at the 20-min time point. Together, the above biomarker results raise the possibility that $Gnat1^{rd17}$ rod mitochondria can increase their oxidation of fuels (suggested by the change in OCR) without undergoing re-distribution at the 20-minute time point. In addition, light-adapted $Gnat1^{rd17}$ mice had a faster rate of fuel oxidation compared to that in the dark per OCR, and greater-than-wildtype biomarkers changes except for the ELM-RPE biomarker, which likely is being influenced by a lack of phototransduction triggered pH-changes in the subretinal space volume.²⁵

Other potential limitations include the inclusion of male and female mice only for the OCT arm of this study (Supplemental Figs. S2, S4); only males were examined by OKT and only females were examined by OCR. However, we found no

impact of sex on the strain-dependent light-dark differences in OCT data; more work is needed to fully address a role of sex in the other arms of the study. Another possible concern is that evidence for an alternative interpretation of band 2 has been proposed based on data collected using a different type of OCT involving adaptive optics; this alternative interpretation seems at odds with data collected using standard OCT and is a topic of controversy.^{87–89} However, at this point, the relevance of this potential alternative interpretation for understanding band 2 measured from OCT data not collected with adaptive optics is unclear. An additional interpretation concern is that outer segment disc shedding can alter outer retina reflectance and begins soon after overnight dark adaptation; the impact of this shedding on our OCT biomarkers requires further investigation.⁹⁰

Clinically, the intensity of OCT ISez band at its maximum value measured from patients is an accepted biomarker of photoreceptor health whose relative reflectance is linked with outer retina neurodegenerative disease severity and degeneration.^{26,28,87,91–94} On the other hand, the relevance of a single value of ISez intensity measured with OCT in relation to mitochondria is unclear, and comparing single intensity measurement between subjects remain challenging in practice because of issues such as a lack of a consensus method for performing intensity normalization.^{26,28,87,91–94}

Intriguingly, Gnat1^{rd17} mice do not show evidence for an HB signal in light or dark (e.g., Fig. 2C). This appears consistent with greater mitochondria activity since a small HB indicates a higher energy condition in different wildtype mouse strains (e.g., Fig. 2B).²⁴ On the other hand, the absence of rod transducin may influence the refractive index of the outer segment making it hard to discern the photoreceptor tips.⁵² A third possibility is that loss of the transducin α subunit function somehow modifies the HB magnitude unrelated to energy production. Unfortunately, at present, the underlying mechanism that produces a prominent HB is unclear and further investigations are required.

Conventional imaging (e.g., positron emission tomography and magnetic resonance imaging) biomarkers are limited by low spatial resolution and indirect evaluation of mitochondria bioenergetics. We have been investigating whether information about mitochondrial activity is encoded in high spatial resolution OCT data. Three rod bioenergetic biomarkers have been identified. The first describes the mitochondria distribution within the rod inner segment ellipsoid as measured by the ISez profile shape. How mitochondria are spatially distributed often determines their ability to respond to a cell's energy requirements.^{95,96} The second is a proxy for mitochondrial-driven/pH-triggered/RPE-water removal from the subretinal space (ELM-RPE) thickness. Summarizing studies performed by several groups using a variety of methods between 1992 and 2017, during dark-adaptation, show rod cGMP accumulates in the outer segment, and this event maintains persistently open cyclic nucleotide-gated channels, an event that depolarizes the rod membrane and increases ion pumping/mitochondrial energy use compared to light adaptation.^{23,24,30–54,97–104} Increased metabolic demand in the dark also stimulates production of more lactate, CO₂ and waste water, each of which acidifies the subretinal space and triggers an increase in apical RPE co-transporter-based water removal with concomitant shrinkage of the ELM-RPE region.²⁵ A third correlate is the HB located between the photoreceptor tips and apical RPE that appears to be pH-independent and associated to thickness of the ELM-

RPE region in wildtype mice.^{24,25,30–34,105} So far, agreement between these three OCT energy biomarkers and conventional assays of mitochondria activity have been found in wildtype mice.

The 2-month Gnat1^{rd17} mice were on a C57BL/6J background and showed OCT evidence for modest rod atrophy which was not found in an earlier histologic study in mice on a ICR background (Fig. 6).^{3,55} In addition, this difference may arise from differences in retinal layer thicknesses measured with both fixed tissue and in vivo, and the unbiased nature of the OCT analysis. In any event, the extent of rod death noted in the present study is not associated with declines in contrast sensitivity and acuity under photopic illumination conditions, consistent with results from other studies in different experimental models.^{106–108} More work is needed to determine if the rod loss noted herein proceeds or predicts the increased rod ISez aspect ratio in vivo.

Somewhat confusingly, a previous study referred to a rod and cone T α double mutant mouse as an “rd17” mouse.¹⁰⁹ However, the mouse strain described in that report appears to have had mutations in both the rod and cone transducin genes. That strain resembles the IRD1 strain and not the Gnat1^{rd17} mouse sold currently by Jackson Laboratories that we used in our study. Our OKT measurements show that the Gnat1^{rd17} strain we used does not have impaired cone function (Fig. 3).^{4,55,109–111} Our OKT results are in line with the reported similarity between Gnat1^{rd17} mice and IRD2 mice that contain nontruncated protein product rod transducin α subunit.^{55,110,111}

Rods have the potential to contribute to the regulation of daytime visual performance, such as contrast sensitivity, by at least three possible mechanisms.^{57,58,77,112} Rods can modify cone function via rod-cone connexin 36 gap junctions.^{113–117} Furthermore, rods alone trigger light-stimulated release of dopamine, a neurotransmitter involved in controlling cone-based vision.^{57,118,119} In addition, a major regulator of the volume of the subretinal space is the rods as shown by the changes in the ELM-RPE thickness in WT mice (Fig. 4). The subretinal space volume is linked with redistribution of key factors involved in proper rod and cone function, such as the interphotoreceptor binding protein.^{30,31,34,57,97,101,112,116,118,120–122} Indeed, underperforming rod mitochondria alone can lead to impaired contrast sensitivity.^{57,77} Thus it is intriguing that the biomarker evidence for rod mitochondria hyperactivity in Gnat1^{rd17} mice was associated with enhanced contrast sensitivity. Also, visual acuity measured by OKT has a large inner retina contribution.⁵⁷ The mitochondria activity in the inner retina of Gnat1^{rd17} mice is unclear at present. Also, it is unclear why INL + OPL region is thicker in Gnat1^{rd17} mice and how this thicker region might have contributed to their greater-than-wildtype acuity; more work is needed to examine these questions.

The effect of constant illumination on consumption of O₂ by isolated Gnat1^{rd17} retinas is transient with OCR being higher in light than in dark for the first 25 minutes (Fig. 7) and then gradually returning to a dark level. For the following reasons, we consider that OCR during the first 25 minutes of light to best represent events in vivo. In the OCR experiment light stimulates consumption of ATP to phosphorylate rhodopsin. Although rhodopsin is readily phosphorylated and dephosphorylated in vivo, it cannot be dephosphorylated in isolated retinas.^{123,124} Also, the isolated retina used in the OCR studies do not contain RPE, and so 11-*cis*-retinal cannot be regenerated for rods. Thus we

reason that after illumination begins, the available pool of rhodopsin eventually becomes phosphorylated and all the 11-*cis*-retinal reduced, so ATP synthesis that initially was required to support rhodopsin phosphorylation declines *ex vivo*. Unfortunately, to our knowledge, there have not been any direct measurements of the time course of rhodopsin phosphorylation under the conditions of the experiment in Figure 7. However, quantification of rhodopsin phosphorylation in mouse retinas *ex vivo* shows that a bright flash stimulus instantaneously bleaches 40% of the rhodopsin and that minutes pass before phosphorylation is complete (Fig. 1 in reference 125). Because the light-stimulus for the experiment in Figure 7 was continuous and much lower intensity (~50% bleach per minute), we speculate that the rate of bleaching would have been relatively slower than after that bright flash. More work is needed to test this hypothesis. Nonetheless, these considerations raise the possibility that phosphorylation in the *ex vivo* preparation would have gone to completion within 25 minutes after the onset of illumination and that the energy consumption would return to the rate that it was in darkness. This is consistent with our observation that OCR returns to the dark level in Gnat1^{rd17} retinas.

Figure 7 also shows the changes in OCR in isolated wild-type retinas. Unlike rd17 mice which lack G-protein signaling in rods, in wildtype mice phototransduction (and its absence in the dark) dominates the overall changes in energy demands in the retina. Light initially stimulates phototransduction and the closure of cyclic GMP-gated ion channels. The slower influx of Na⁺ and Ca²⁺ diminishes the demand for ATP hydrolysis to pump those ions out of the cell. When opsin in wildtype retinas becomes completely phosphorylated in response to photoactivation and when there is no 11-*cis* retinal to regenerate it to rhodopsin, the phosphorylated opsin will bind arrestin and become ineffective, but not 100% quenched, in its ability to stimulate transducin (which cannot happen in Gnat1^{rd17} mice).¹²⁶ Under these conditions, much less hydrolysis of cyclic GMP takes place, and guanylyl cyclase will resynthesize cyclic GMP, raising the steady-state cyclic GMP concentration and reopening some of the cGMP-gated channels in the rod outer segments. That will cause an increase in Na⁺ influx, which will increase energy demand by requiring a corresponding pumping of Na⁺ out of the cell by the Na/K ATPase. This increase in ATP demand (and O₂ consumption) should offset the decrease in ATP demand that is associated with the decrease usage of ATP for rhodopsin phosphorylation. Overall, there is a very large change in energy between light and dark that relies on transducin in wildtype retinas. The absence of that change in the Gnat1^{rd17} retina reveals the impact of other energy consuming processes.

In summary, the present OCT and OCR biomarker data together raise the possibility, for the first time, of greater rod mitochondria activity during illumination in Gnat1^{rd17} retinas than in the dark, an abnormal physiology that occurred with modest rod loss *in vivo*.⁴ Light-adapted Gnat1^{rd17} mice cones were functional, and the impression from all biomarker data is of a higher-than-normal energy demand in rods that appeared sustained via distinct mitochondrial mechanisms. It seems likely that the present biomarker evidence for rod mitochondria overperformance may involve the “dark” current and an additional demand for energy linked to ongoing rhodopsin phosphorylation and visual cycle activity. More work is needed to determine whether rod mitochondria activity and atrophy of rods in Gnat1^{rd17} retinas are causally linked. Nonetheless, the present data raise the

possibility of using OCT to test new therapeutic approaches that could influence mitochondria activity early in the course of inherited rod degeneration due to loss of function in transducin 1 and likely other mutations.^{39–42,44–51}

Acknowledgments

The authors thank Vladimir Kefalov for a helpful discussion regarding the interpretation of the OCR data.

Supported by the National Institutes of Health (EY026584 [B.A.B.], AG058171 [B.A.B.], EY06641 [J.B.H.], EY017863 [J.B.H.], and EY032597 [J.B.H.]), NIH intramural Research Programs (EY000503 [H.Q.], EY000530 [H.Q.]), NEI Core Grant P30 (EY04068), and an unrestricted grant from Research to Prevent Blindness (Kresge Eye Institute, B.A.B.).

Disclosure: **B.A. Berkowitz**, None; **R.H. Podolsky**, None; **K.L. Childers**, None; **R. Roberts**, None; **R. Katz**, None; **R. Waseem**, None; **B.M. Robbins**, None; **D.T. Hass**, None; **J.B. Hurley**, None; **I.R. Sweet**, None; **C. Goodman**, None; **H. Qian**, None; **B. Alvisio**, None; **S. Heaps**, None

References

- Calvert PD, Krasnoperova NV, Lyubarsky AL, et al. Phototransduction in transgenic mice after targeted deletion of the rod transducin alpha -subunit. *Proc Natl Acad Sci USA*. 2000;97:13913–13918.
- Carrigan M, Duignan E, Humphries P, Palfi A, Kenna PF, Farrar GJ. A novel homozygous truncating *GNAT1* mutation implicated in retinal degeneration. *Br J Ophthalmol*. 2016;100:495–500.
- Miyamoto M, Aoki M, Sugimoto S, Kawasaki K, Imai R. IRD1 and IRD2 mice, naturally occurring models of hereditary retinal dysfunction, show late-onset and progressive retinal degeneration. *Current Eye Research*. 2010;35:137–145.
- Collin GB, Gogna N, Chang B, et al. Mouse models of inherited retinal degeneration with photoreceptor cell loss. *Cells*. 2020;9:931.
- Gopalakrishnan S, Mehrvar S, Maleki S, et al. Photobiomodulation preserves mitochondrial redox state and is retinoprotective in a rodent model of retinitis pigmentosa. *Scientific Reports*. 2020;10:1–13.
- Zenteno JC, García-Montaña LA, Cruz-Aguilar M, et al. Extensive genic and allelic heterogeneity underlying inherited retinal dystrophies in Mexican patients molecularly analyzed by next-generation sequencing. *Mol Genet Genomic Med*. 2020;8:10.1002/mgg3.1044.
- Zeitz C, Méjécase C, Stévenard M, Michiels C, Audo I, Marmor MF. A novel heterozygous missense mutation in *GNAT1* leads to autosomal dominant Riggs type of congenital stationary night blindness. *Biomed Res Int*. 2018;2018:7694801.
- Kim HM, Joo K, Han J, Woo SJ. Clinical and genetic characteristics of Korean congenital stationary night blindness patients. *Genes (Basel)*. 2021;12:789.
- Méjécase C, Laurent-Coriat C, Mayer C, et al. Identification of a Novel Homozygous Nonsense Mutation Confirms the Implication of *GNAT1* in Rod-Cone Dystrophy. *PLoS One*. 2016;11:e0168271.
- Hartong DT, Berson EL, Dryja TP. Retinitis pigmentosa. *Lancet*. 2006;368:1795–1809.
- McLaughlin ME, Sandberg MA, Berson EL, Dryja TP. Recessive mutations in the gene encoding the beta-subunit of rod phosphodiesterase in patients with retinitis pigmentosa. *Nat Genet*. 1993;4:130–134.
- Gal A, Orth U, Baehr W, Schwinger E, Rosenberg T. Heterozygous missense mutation in the rod cGMP

- phosphodiesterase beta-subunit gene in autosomal dominant stationary night blindness. *Nat Genet.* 1994;7:64–68.
13. Berkowitz BA, Podolsky RH, Childers KL, et al. Rod Photoreceptor Neuroprotection in Dark-Reared Pde6brd10 Mice. *Invest Ophthalmol Vis Sci.* 2020;61:14–14.
 14. Berkowitz BA, Podolsky RH, Berri AM, et al. Dark rearing does not prevent rod oxidative stress in vivo in Pde6brd10 mice. *Invest Ophthalmol Vis Sci.* 2018;59:1659–1665.
 15. Jiang K, Mondal AK, Adlakha YK, et al. Multiomics analyses reveal early metabolic imbalance and mitochondrial stress in neonatal photoreceptors leading to cell death in Pde6brd1/rd1 mouse model of retinal degeneration. *Hum Mol Genet.* 2022;31:2137–2154.
 16. Zhou J, Rasmussen M, Ekström P. cGMP-PKG dependent transcriptome in normal and degenerating retinas: novel insights into the retinitis pigmentosa pathology. *Exp Eye Res.* 2021;212:108752.
 17. Perron NR, Beeson C, Rohrer B. Early alterations in mitochondrial reserve capacity; a means to predict subsequent photoreceptor cell death. *J Bioenerg Biomembr.* 2013;45:101–109.
 18. Fain GL. Why photoreceptors die (and why they don't). *Bioessays.* 2006;28:344–354.
 19. Vinberg F, Chen J, Kefalov VJ. Regulation of calcium homeostasis in the outer segments of rod and cone photoreceptors. *Prog Retinal Eye Res.* 2018;67:87–101.
 20. Acosta ML, Shin Y-S, Ready S, Fletcher EL, Christie DL, Kalloniatis M. Retinal metabolic state of the proline-23-histidine rat model of retinitis pigmentosa. *Am J Physiol Cell Physiol.* 2010;298:C764–C774.
 21. Acosta ML, Fletcher EL, Azizoglu S, Foster LE, Farber DB, Kalloniatis M. Early markers of retinal degeneration in rd/rd mice. *Mol Vis.* 2005;11:717–728.
 22. Lim JKH, Li QX, He Z, et al. Retinal functional and structural changes in the 5xFAD mouse model of Alzheimer's disease. *Front Neurosci.* 2020;14:862.
 23. Berkowitz BA, Podolsky RH, Childers KL, et al. Functional changes within the rod inner segment ellipsoid in wild-type mice: an optical coherence tomography and electron microscopy study. *Invest Ophthalmol Vis Sci.* 2022;63:8–8.
 24. Gao S, Li Y, Bissig D, et al. Functional regulation of an outer retina hyporeflexive band on optical coherence tomography images. *Sci Rep.* 2021;11:10260.
 25. Berkowitz BA, Qian H. OCT imaging of rod mitochondrial respiration in vivo. *Exp Biol Medicine (Maywood).* 2021;246:2151–2158.
 26. Staurengi G, Sadda S, Chakravarthy U, Spaide RF. Proposed lexicon for anatomic landmarks in normal posterior segment spectral-domain optical coherence tomography: the IN•OCT consensus. *Ophthalmology.* 2014;121:1572–1578.
 27. Spaide RF. Outer retinal bands. *Invest Ophthalmol Vis Sci.* 2015;56:2505–2506.
 28. Spaide RF, Curcio CA. Anatomical correlates to the bands seen in the outer retina by optical coherence tomography: literature review and model. *Retina.* 2011;31:1609–1619.
 29. Litts KM, Zhang Y, Freund KB, Curcio CA. Optical coherence tomography and histology of age-related macular degeneration support mitochondria as reflectivity sources. *Retina.* 2018;38:445–461.
 30. Bissig D, Berkowitz BA. Light-dependent changes in outer retinal water diffusion in rats in vivo. *Mol Vis.* 2012;18:2561–2562.xxx.
 31. Berkowitz BA, Grady EM, Khetarpal N, Patel A, Roberts R. Oxidative stress and light-evoked responses of the posterior segment in a mouse model of diabetic retinopathy. *Invest Ophthalmol Vis Sci.* 2015;56:606–615.
 32. Berkowitz BA, Olds HK, Richards C, et al. Novel imaging biomarkers for mapping the impact of mild mitochondrial uncoupling in the outer retina in vivo. *PLOS ONE.* 2020;15:e0226840.
 33. Berkowitz BA, Podolsky RH, Qian H, et al. Mitochondrial respiration in outer retina contributes to light-evoked increase in hydration in vivo. *Invest Ophthalmol Vis Sci.* 2018;59:5957–5964.
 34. Li Y, Fariss RN, Qian JW, Cohen ED, Qian H. Light-induced thickening of photoreceptor outer segment layer detected by ultra-high resolution OCT imaging. *Invest Ophthalmol Vis Sci.* 2016;57:Oct105–Oct111.
 35. Zhang J, Gao F, Ma Y, Xue T, Shen Y. Identification of early-onset photoreceptor degeneration in transgenic mouse models of Alzheimer's disease. *iScience.* 2021;24:103327.
 36. Zhang M, Zhong L, Han X, et al. Brain and retinal abnormalities in the 5xFAD mouse model of Alzheimer's disease at early stages. *Front Neurosci.* 2021;15:681831.
 37. Kim S, Yun HM, Baik JH, Chung KC, Nah SY, Rhim H. Functional interaction of neuronal Cav1.3 L-type calcium channel with ryanodine receptor type 2 in the rat hippocampus. *J Biol Chem.* 2007;282:32877–32889.
 38. Berkowitz BA, Podolsky RH, Farrell B, et al. D-cis-diltiazem can produce oxidative stress in healthy depolarized rods in vivo. *Invest Ophthalmol Vis Sci.* 2018;59:2999–3010.
 39. Chakroborty S, Briggs C, Miller MB, et al. Stabilizing ER Ca2+ channel function as an early preventative strategy for Alzheimer's disease. *PLoS One.* 2012;7:e52056.
 40. McDaid J, Mustaly-Kalimi S, Stutzmann GE. Ca(2+) dyshomeostasis disrupts neuronal and synaptic function in Alzheimer's disease. *Cells.* 2020;9:2655.
 41. Yao J, Liu Y, Sun B, et al. Increased RyR2 open probability induces neuronal hyperactivity and memory loss with or without Alzheimer's disease-causing gene mutations. *Alzheimers Dement.* 2022;18:2088–2098.
 42. Yao J, Sun B, Institoris A, et al. Limiting RyR2 open time prevents Alzheimer's disease-related neuronal hyperactivity and memory loss but not β -amyloid accumulation. *Cell Rep.* 2020;32:108169.
 43. Huang W, Xing W, Ryskamp DA, Punzo C, Kri++aj D. Localization and phenotype-specific expression of ryanodine calcium release channels in C57BL6 and DBA/2J mouse strains. *Exp Eye Res.* 2011;93:700–709.
 44. Paula-Lima AC, Adasme T, SanMartín C, et al. Amyloid β -peptide oligomers stimulate RyR-mediated Ca2+ release inducing mitochondrial fragmentation in hippocampal neurons and prevent RyR-mediated dendritic spine remodeling produced by BDNF. *Antioxid Redox Signal.* 2011;14:1209–1223.
 45. Hwang K-D, Bak MS, Kim SJ, Rhee S, Lee Y-S. Restoring synaptic plasticity and memory in mouse models of Alzheimer's disease by PKR inhibition. *Mol Brain.* 2017;10:57.
 46. Shi Y, Zhang L, Gao X, et al. Intranasal dantrolene as a disease-modifying drug in Alzheimer 5XFAD mice. *J Alzheimers Dis.* 2020;76:1375–1389.
 47. Lerdkrai C, Asavapanumas N, Brawek B, et al. Intracellular Ca(2+) stores control in vivo neuronal hyperactivity in a mouse model of Alzheimer's disease. *Proc Natl Acad Sci USA.* 2018;115:E1279–E1288.
 48. Hector A, Brouillette J. Hyperactivity induced by soluble amyloid- β oligomers in the early stages of Alzheimer's disease. *Frontiers in Molecular Neuroscience.* 2021;13:600084.
 49. Hascup KN, Findley CA, Britz J, et al. Riluzole attenuates glutamatergic tone and cognitive decline in A β PP/PS1 mice. *J Neurochem.* 2021;156:513–523.

50. Nakamura Y, Yamamoto T, Xu X, et al. Enhancing calmodulin binding to ryanodine receptor is crucial to limit neuronal cell loss in Alzheimer disease. *Sci Rep.* 2021;11:7289.
51. Habiba U, Descallar J, Kreilau F, et al. Detection of retinal and blood A β oligomers with nanobodies. *Alzheimers Dement.* 2021;13:e12193.
52. Zhang P, Zawadzki RJ, Goswami M, et al. In vivo optophysiology reveals that G-protein activation triggers osmotic swelling and increased light scattering of rod photoreceptors. *Proc Natl Acad Sci USA.* 2017;114:E2937–E2946.
53. Zhang F, Kurokawa K, Lassoued A, Crowell JA, Miller DT. Cone photoreceptor classification in the living human eye from photostimulation-induced phase dynamics. *Proc Natl Acad Sci USA.* 2019;116:7951–7956.
54. Lassoued A, Zhang F, Kurokawa K, et al. Cone photoreceptor dysfunction in retinitis pigmentosa revealed by optoretinography. *Proc Natl Acad Sci USA.* 2021;118(47):e2107444118.
55. Stofkova A, Zloh M, Andreanska D, et al. Depletion of retinal dopaminergic activity in a mouse model of rod dysfunction exacerbates experimental autoimmune uveoretinitis: a role for the gateway reflex. *Int J Mol Sci.* 2021;23:453.
56. Berkowitz BA, Podolsky RH, Lins Childers K, et al. Sildenafil-evoked photoreceptor oxidative stress in vivo is unrelated to impaired visual performance in mice. *PLoS One.* 2021;16:e0245161.
57. Jackson CR, Ruan GX, Aseem F, et al. Retinal dopamine mediates multiple dimensions of light-adapted vision. *J Neurosci.* 2012;32:9359–9368.
58. Cahill H, Nathans J. The optokinetic reflex as a tool for quantitative analyses of nervous system function in mice: application to genetic and drug-induced variation. *PLoS ONE.* 2008;3:e2055.
59. Liu H, Tang J, Du Y, et al. Transducin1, phototransduction and the development of early diabetic retinopathy. *Invest Ophthalmol Vis Sci.* 2019;60:1538–1546.
60. Berkowitz BA, Podolsky RH, Lins-Childers KM, Li Y, Qian H. Outer retinal oxidative stress measured in vivo using QUEEnch-assISTed (QUEST) OCT. *Invest Ophthalmol Vis Sci.* 2019;60:1566–1570.
61. Prusky GT, Alam NM, Beekman S, Douglas RM. Rapid quantification of adult and developing mouse spatial vision using a virtual optomotor system. *Invest Ophthalmol Vis Sci.* 2004;45:4611–4616.
62. Douglas RM, Alam NM, Silver BD, McGill TJ, Tschetter WW, Prusky GT. Independent visual threshold measurements in the two eyes of freely moving rats and mice using a virtual-reality optokinetic system. *Vis Neurosci.* 2005;22:677–684.
63. Berkowitz BA, Grady EM, Roberts R. Confirming a prediction of the calcium hypothesis of photoreceptor aging in mice. *Neurobiol Aging.* 2014;35:1883–1891.
64. Ortin-Martinez A, Nadal-Nicolas FM, Jimenez-Lopez M, et al. Number and distribution of mouse retinal cone photoreceptors: differences between an albino (Swiss) and a pigmented (C57/BL6) strain. *PLoS One.* 2014;9:e102392.
65. Applebury ML, Antoch MP, Baxter LC, et al. The murine cone photoreceptor: a single cone type expresses both S and M opsins with retinal spatial patterning. *Neuron.* 2000;27:513–523.
66. Pandiyan VP, Maloney-Bertelli A, Kuchenbecker JA, et al. The optoretinogram reveals the primary steps of phototransduction in the living human eye. *Sci Adv.* 2020;6(37):eabc1124.
67. Bizheva K, Pflug R, Hermann B, et al. Optophysiology: depth-resolved probing of retinal physiology with functional ultrahigh-resolution optical coherence tomography. *Proc Natl Acad Sci USA.* 2006;103:5066–5071.
68. Gao S, Zeng Y, Li Y, Cohen ED, Berkowitz BA, Qian H. Fast and slow light-induced changes in murine outer retina OCT: complimentary high spatial resolution functional biomarkers. *PNAS Nexus.* 2022;1(4):pgac208.
69. Ronneberger O, Fischer P, Brox T. U-net: Convolutional networks for biomedical image segmentation. In: *International Conference on Medical image computing and computer-assisted intervention.* Cham: Springer; 2015:234–241.
70. Kugelman J, Alonso-Caneiro D, Read SA, et al. Automatic choroidal segmentation in OCT images using supervised deep learning methods. *Sci Rep.* 2019;9:1–13.
71. Schneider CA, Rasband WS, Eliceiri KW. NIH Image to ImageJ: 25 years of image analysis. *Nat Methods.* 2012;9:671–675.
72. Mulchrone KF, Choudhury KR. Fitting an ellipse to an arbitrary shape: implications for strain analysis. *J Structural Geology.* 2004;26:143–153.
73. DeRamus ML, Stacks DA, Zhang Y, Huisingh CE, McGwin G, Pittler SJ. GARP2 accelerates retinal degeneration in rod cGMP-gated cation channel β -subunit knockout mice. *Sci Rep.* 2017;7:42545.
74. Soukup P, Maloca P, Altmann B, Festag M, Atzpodien EA, Pot S. Interspecies Variation of Outer Retina and Choriocapillaris Imaged With Optical Coherence Tomography. *Invest Ophthalmol Vis Sci.* 2019;60:3332–3342.
75. Zhang T, Kho AM, Yiu G, Srinivasan VJ. Visible light optical coherence tomography (OCT) quantifies subcellular contributions to outer retinal band 4. *Transl Vis Sci Technol.* 2021;10:30–30.
76. Berkowitz BA, Podolsky RH, Childers KL, et al. Correcting QUEST magnetic resonance imaging–sensitive free radical production in the outer retina in vivo does not correct reduced visual performance in 24-month-old C57BL/6J mice. *Invest Ophthalmol Vis Sci.* 2021;62:24–24.
77. Berkowitz BA, Podolsky RH, Lenning J, et al. Sodium iodate produces a strain-dependent retinal oxidative stress response measured in vivo using QUEST MRI. *Invest Ophthalmol Vis Sci.* 2017;58:3286–3293.
78. Berkowitz BA, Lewin AS, Biswal MR, Bredell BX, Davis C, Roberts R. MRI of retinal free radical production with laminar resolution in vivo. *Invest Ophthalmol Vis Sci.* 2016;57:577–585.
79. Berkowitz BA, Bredell BX, Davis C, Samardzija M, Grimm C, Roberts R. Measuring in vivo free radical production by the outer retina. *Invest Ophthalmol Vis Sci.* 2015;56:7931–7938.
80. Medrano CJ, Fox DA. Oxygen consumption in the rat outer and inner retina: light- and pharmacologically-induced inhibition. *Exp Eye Res.* 1995;61:273–284.
81. Kooragayala K, Gotoh N, Cogliati T, et al. Quantification of oxygen consumption in retina ex vivo demonstrates limited reserve capacity of photoreceptor mitochondria. *Invest Ophthalmol Vis Sci.* 2015;56:8428–8436.
82. Kamat V, Robbings BM, Jung SR, et al. Fluidics system for resolving concentration-dependent effects of dissolved gases on tissue metabolism. *Elife.* 2021;10:e66716.
83. Bisbach CM, Hass DT, Robbings BM, et al. Succinate can shuttle reducing power from the hypoxic retina to the O(2)-rich pigment epithelium. *Cell Rep.* 2020;31:107606.
84. Sweet IR, Khalil G, Wallen AR, et al. Continuous measurement of oxygen consumption by pancreatic islets. *Diabetes Technol Ther.* 2002;4:661–672.
85. Meschede IP, Ovenden NC, Seabra MC, et al. Symmetric arrangement of mitochondria:plasma membrane contacts between adjacent photoreceptor cells regulated by Opa1. *Proc Natl Acad Sci.* 2020;117:15684–15693.
86. Kam JH, Jeffery G. To unite or divide: mitochondrial dynamics in the murine outer retina that preceded age related photoreceptor loss. *Oncotarget.* 2015;6:26690–26701.

87. Jonnal RS, Kocaoglu OP, Zawadzki RJ, Lee S-H, Werner JS, Miller DT. The cellular origins of the outer retinal bands in optical coherence tomography images. *Invest Ophthalmol Vis Sci.* 2014;55:7904–7918.
88. Chauhan P, Kho AM, FitzGerald P, Shibata B, Srinivasan VJ. Subcellular comparison of visible-light optical coherence tomography and electron microscopy in the mouse outer retina. *Invest Ophthalmol Vis Sci.* 2022;63:10–10.
89. Yao X, Son T, Kim TH, Le D. Interpretation of anatomic correlates of outer retinal bands in optical coherence tomography. *Exp Biol Med (Maywood).* 2021;246:2140–2150.
90. Kocaoglu OP, Liu Z, Zhang F, Kurokawa K, Jonnal RS, Miller DT. Photoreceptor disc shedding in the living human eye. *Biomed Opt Express.* 2016;7:4554–4568.
91. Lee KE, Heitkotter H, Carroll J. Challenges associated with ellipsoid zone intensity measurements using optical coherence tomography. *Transl Vis Sci Technol.* 2021;10:27.
92. Schaal KB, Rosenfeld PJ. The Controversy of Band# 2. 2018.
93. Cai CX, Locke KG, Ramachandran R, Birch DG, Hood DC. A comparison of progressive loss of the ellipsoid zone (EZ) band in autosomal dominant and x-linked retinitis pigmentosa. *Invest Ophthalmol Vis Sci.* 2014;55:7417–7422.
94. Sassmannshausen M, Behning C, Isselmann B, et al. Relative ellipsoid zone reflectivity and its association with disease severity in age-related macular degeneration: a MACUSTAR study report. *Sci Rep.* 2022;12:1–12.
95. Seager R, Lee L, Henley JM, Wilkinson KA. Mechanisms and roles of mitochondrial localisation and dynamics in neuronal function. *Neuronal Signal.* 2020;4:Ns20200008.
96. Sun N, Finkel T. Cardiac mitochondria: a surprise about size. *J Mol Cell Cardiol.* 2015;82:213–215.
97. Adijanto J, Banzon T, Jalickee S, Wang NS, Miller SS. CO₂-induced ion and fluid transport in human retinal pigment epithelium. *J Gen Physiol.* 2009;133:603–622.
98. Berkowitz BA, Bissig D, Roberts R. MRI of rod cell compartment-specific function in disease and treatment in vivo. *Prog Retin Eye Res.* 2016;51:90–106.
99. Hamann S, Kiilgaard JF, la Cour M, Prause JU, Zeuthen T. Cotransport of H⁺, lactate, and H₂O in porcine retinal pigment epithelial cells. *Exp Eye Res.* 2003;76:493–504.
100. Lu CD, Lee B, Schottenhamml J, Maier A, Pugh EN, Fujimoto JG. Photoreceptor layer thickness changes during dark adaptation observed with ultrahigh-resolution optical coherence tomography. *Invest Ophthalmol Vis Sci.* 2017;58:4632–4643.
101. Li JD, Govardovskii VI, Steinberg RH. Light-dependent hydration of the space surrounding photoreceptors in the cat retina. *Vis Neurosci.* 1994;11:743–752.
102. Govardovskii VI, Li JD, Dmitriev AV, Steinberg RH. Mathematical model of TMA⁺ diffusion and prediction of light-dependent subretinal hydration in chick retina. *Invest Ophthalmol Vis Sci.* 1994;35:2712–2724.
103. Li JD, Gallemore RP, Dmitriev A, Steinberg RH. Light-dependent hydration of the space surrounding photoreceptors in chick retina. *Invest Ophthalmol Vis Sci.* 1994;35:2700–2711.
104. Huang B, Karwoski CJ. Light-evoked expansion of subretinal space volume in the retina of the frog. *J Neurosci.* 1992;12:4243–4252.
105. Yamamoto F, Steinberg RH. Effects of intravenous acetazolamide on retinal pH in the cat. *Exp Eye Res.* 1992;54:711–718.
106. McGill TJ, Prusky GT, Douglas RM, et al. Discordant anatomical, electrophysiological, and visual behavioral profiles of retinal degeneration in rat models of retinal degenerative disease. *Invest Ophthalmol Vis Sci.* 2012;53:6232–6244.
107. Alves CH, Boon N, Mulder AA, Koster AJ, Jost CR, Wijnholds J. CRB2 loss in rod photoreceptors is associated with progressive loss of retinal contrast sensitivity. *Int J Mol Sci.* 2019;20:4069.
108. Cuenca N, Fernández-Sánchez L, Sauvé Y, et al. Correlation between SD-OCT, immunocytochemistry and functional findings in an animal model of retinal degeneration. *Front Neuroanat.* 2014;8:151.
109. Deng W-T, Sakurai K, Liu J, et al. Functional interchangeability of rod and cone transducin α -subunits. *Proc Natl Acad Sci.* 2009;106:17681–17686.
110. Miyamoto M, Imai R, Sugimoto S, Aoki M, Nagai H, Ando T. Visual electrophysiological features of two naturally occurring mouse models with retinal dysfunction. *Curr Eye Res.* 2006;31:329–335.
111. Miyamoto M, Aoki M, Hirai K, Sugimoto S, Kawasaki K, Imai R. A nonsense mutation in Gnat1, encoding the alpha subunit of rod transducin, in spontaneous mouse models of retinal dysfunction. *Exp Eye Res.* 2010;90:63–69.
112. Jeon CJ, Strettoi E, Masland RH. The major cell populations of the mouse retina. *J Neurosci.* 1998;18:8936–8946.
113. O'Brien JJ, Chen X, Macleish PR, O'Brien J, Massey SC. Photoreceptor coupling mediated by connexin36 in the primate retina. *J Neurosci.* 2012;32:4675–4687.
114. Abd-El-Barr MM, Pennesi ME, Saszik SM, et al. Genetic dissection of rod and cone pathways in the dark-adapted mouse retina. *J Neurophysiol.* 2009;102:1945–1955.
115. Deans MR, Volgyi B, Goodenough DA, Bloomfield SA, Paul DL. Connexin36 is essential for transmission of rod-mediated visual signals in the mammalian retina. *Neuron.* 2002;36:703–712.
116. Gldenagel M, Ammermiller J, Feigenspan A, et al. Visual transmission deficits in mice with targeted disruption of the gap junction gene Connexin36. *J Neurosci.* 2001;21:6036–6044.
117. Jin N, Zhang Z, Keung J, et al. Molecular and functional architecture of the mouse photoreceptor network. *Sci Adv.* 2020;6:eaba7232.
118. Pérez-Fernández V, Milosavljevic N, Allen AE, et al. Rod photoreceptor activation alone defines the release of dopamine in the retina. *Curr Biol.* 2019;29:763–774.e765.
119. Aung MH, Hn Park, Han MK, et al. Dopamine deficiency contributes to early visual dysfunction in a rodent model of type 1 diabetes. *J Neurosci.* 2014;34:726–736.
120. Asteriti S, Gargini C, Cangiano L. Mouse rods signal through gap junctions with cones. *Elife.* 2014;3:e01386.
121. Baldrige WH, Vaney DI, Weiler R. The modulation of intercellular coupling in the retina. *Semin Cell Dev Biol.* 1998;9:311–318.
122. Roy S, Field GD. Dopaminergic modulation of retinal processing from starlight to sunlight. *J Pharmacol Sci.* 2019;140:86–93.
123. Berry J, Frederiksen R, Yao Y, Nymark S, Chen J, Cornwall C. Effect of rhodopsin phosphorylation on dark adaptation in mouse rods. *J Neurosci.* 2016;36:6973–6987.
124. Lee KA, Nawrot M, Garwin GG, Saari JC, Hurley JB. Relationships among visual cycle retinoids, rhodopsin phosphorylation, and phototransduction in mouse eyes during light and dark adaptation. *Biochemistry.* 2010;49:2454–2463.
125. Kennedy MJ, Lee KA, Niemi GA, et al. Multiple phosphorylation of rhodopsin and the in vivo chemistry underlying rod photoreceptor dark adaptation. *Neuron.* 2001;31:87–101.
126. Sampath AP, Matthews HR, Cornwall MC, Fain GL. Bleached pigment produces a maintained decrease in outer segment Ca²⁺ in salamander rods. *J Gen Physiol.* 1998;111:53–64.